

1 **Navigational strategies underlying temporal phototaxis in *Drosophila* larvae**

2 Maxwell L. Zhu^{1,2}, Kristian J. Herrera², Katrin Vogt^{1,3}, and Armin Bahl^{2,3,4,*}

3

4 ¹Department of Physics, Harvard University, Cambridge, MA, USA

5 ²Department of Molecular and Cellular Biology, Harvard University, Cambridge, MA, USA

6 ³Department of Biology, University of Konstanz, Konstanz, Germany

7 ⁴Centre for the Advanced Study of Collective Behaviour, University of Konstanz, Konstanz, Germany

8

9 *Correspondence: armin.bahl@uni-konstanz.de

10

11 Keywords: *Drosophila* larvae, animal behavior, posture tracking, navigation, phototaxis, modeling

12

13 Summary statement: 38 words

14 Abstract: 131 words

15 Introduction: 310 words

16 Materials and methods: 1920 words

17 Results and discussion: 1715 words

18 Figure legends: 491 words

19 Total (introduction, materials and methods, results and discussion, and figure legends): **2516 words**

20 References: 24

21

22 **Summary statement**

23 Using a novel closed-loop behavioral assay, we show that *Drosophila* larvae can navigate light
24 gradients exclusively using temporal cues. Analyzing and modeling their behavior in detail, we
25 propose that larvae achieve this by integrating brightness change during runs.

26

27 **Abstract**

28 Navigating across light gradients is essential for survival for many animals. However, we still
29 have a poor understanding of the algorithms that underlie such behaviors. Here we develop a
30 novel phototaxis assay for *Drosophila* larvae in which light intensity is always spatially uniform
31 but updates depending on the location of the animal in the arena. Even though larvae can only
32 rely on temporal cues in this closed-loop setup, we find that they are capable of finding
33 preferred areas of low light intensity. Further detailed analysis of their behavior reveals that
34 larvae turn more frequently and that heading angle changes increase when they experience
35 brightness increments over extended periods of time. We suggest that temporal integration of
36 brightness change during runs is an important – and so far largely unexplored – element of
37 phototaxis.

38

39 Introduction

40 Many animals have evolved behaviors to find favorable locations in complex natural
41 environments. Such behaviors include chemotaxis to approach or avoid chemical stimuli;
42 thermotaxis to find cooler or warmer regions; and phototaxis to approach or avoid light (Gepner
43 et al., 2015; Gomez-Marin and Louis, 2014; Gomez-Marin et al., 2011; Kane et al., 2013; Klein
44 et al., 2015; Luo et al., 2010).

45 *Drosophila* larvae are negatively phototactic, preferring darker regions (Sawin et al., 1994).
46 To navigate, larvae alternate between runs and turns. During runs, larvae move relatively
47 straight. During turns, they slow down and perform head-casts (Lahiri et al., 2011) to sample
48 their environment for navigational decisions (Gomez-Marin and Louis, 2012; Humberg and
49 Sprecher, 2018; Humberg et al., 2018; Kane et al., 2013). However, it is unclear whether such
50 local spatial sampling is necessary to perform phototaxis. Zebrafish larvae, for example, can
51 perform phototaxis even when light intensity is uniform across space but changes over time with
52 the animal's position (Chen and Engert, 2014). In a purely temporal phototaxis assay, spatial
53 information is absent, so navigation must depend on other cues.

54 Previous work indicates that as brightness increases, *Drosophila* larvae make shorter runs
55 and bigger turns (Humberg et al., 2018; Kane et al., 2013). This is reminiscent of chemotactic
56 strategies, where decreasing concentrations of a favorable odorant increase the likelihood of
57 turning (Gomez-Marin et al., 2011). While it has been shown that temporal sampling of olfactory
58 cues is sufficient to guide chemotaxis (Schulze et al., 2015), it remains unclear whether larvae
59 can use a purely temporal strategy for visual navigation.

60 Using a virtual landscape in which brightness is always spatially uniform but depends on the
61 location of the animal in the arena, we confirm that larvae can perform phototaxis by modulating
62 run-length and heading angle. Our data indicate that larvae achieve this by integrating
63 brightness change during runs (**Video S1**).

64

65 **Materials and methods**

66

67 Experimental setup

68 All experiments were performed using wild-type 2nd-instar *Drosophila melanogaster* larvae
69 collected 3–4 days after egg-laying. This age was chosen to ensure consistent phototactic
70 behavior because older larvae might change their light preference (Sawin-McCormack et al.,
71 1995). Larvae were raised on agarose plates with grape juice and yeast paste, with a 12h/12h
72 light-dark cycle at 22°C and 60% humidity. Before experiments, larvae were washed in droplets
73 of deionized water. All experiments were carried out between 2 pm and 7 pm to avoid potential
74 circadian effects (Mazzoni et al., 2005). Each experiment lasted for 60 min. For all stimuli,
75 animals were presented with constant gray during the first 15 min, allowing them to distribute in
76 the arena.

77 Larvae were placed in the center of a custom-made circular acrylic dish (6 cm radius) filled
78 with a thin layer of freshly made 2% agarose (**Fig. 1A**). As previously described (Bahl and
79 Engert, 2020), spatially uniform whole-field illumination was presented via a projector (60 Hz,
80 AAXA P300 Pico Projector) from below. Brightness was set by the computer and ranged from
81 values 0 to 255. Respective light intensity was measured using an Extech Instruments Light
82 Meter LT300 and ranged from 41 Lux to 2870 Lux (**Fig. S1A**). We did not attempt to linearize
83 this curve as it is unclear how the larval visual system processes contrast. Therefore, for all
84 brightness-dependent behavioral analyses, the original pixel brightness value, as set by the
85 program, was used.

86 Three virtual light intensity landscapes were tested: a “Valley” stimulus, a “Ramp” stimulus,
87 and a “Constant” stimulus. For the “Valley” and “Ramp” stimuli, the spatially uniform light
88 brightness (λ) was updated in closed-loop according to $\lambda = 255 \cdot (r - 3)^2 / 9$ (**Figs. 1B** and **S2A**)
89 and $\lambda = 255 \cdot (1 - \sqrt{1 - r/6})$ (**Fig. S3A**), respectively, where r is the larva’s radial distance to
90 the center of the arena. Both profiles ensure that brightness levels near the wall are high,
91 decreasing the edge preference of larvae and reducing boundary effects. For the “Constant”
92 stimulus, brightness values remained gray ($\lambda = 128$) regardless of the larva’s position.

93 For online tracking, the scene was illuminated using infrared LED panels (940 nm panel, 15-
94 IL05, Cop Security). A high-speed camera (90 Hz, USB3 Grasshopper3-NIR, FLIR Systems)
95 with an infrared filter (R72, Hoya) was used to track the larva’s centroid position in real-time.
96 Eight independent arenas were operated in parallel, making the system medium to high-

97 throughput and relatively cost-effective. The position of the animal was determined by spatially
98 filtering the background-subtracted image and then searching for the largest contour. The
99 procedure provides a reliable estimate of the animal's centroid position but cannot determine
100 the precise location of the head or the tail. Using the centroid as a closed-loop position signal
101 significantly simplifies the experimental procedure and is justified as larvae are small in size
102 relative to the slowly changing and always spatially uniform virtual brightness landscapes. The
103 spatial precision of our tracking was in the order of ± 0.01 cm per ~ 10 ms, resulting in a nearly
104 noise-free presentation of the stimulus profiles (**Fig. S1B**). In addition to the online-tracking, a
105 video of the animal was stored for offline posture analysis (**Video S2**).

106 In our system, the closed-loop latency between the detection of the animal's position and
107 the update of the visual stimulus is 100 ms. This value was determined using the following
108 protocol: Infrared filters were removed from the cameras, allowing for direct measurements of
109 the brightness from the projector. Arena brightness starts at a high level but is set to a dark
110 state after a few seconds. When the camera detects such an event, the computer sets the
111 brightness back at a high level. The length of the resulting dark period is the closed-loop delay.
112 Using this strategy, the resulting value contains the sum of all delays of the system (camera
113 image acquisition, image buffering, data transport to the USB 3.0 hub, PCI-express to CPU
114 transport, CPU image analysis, command to the graphics card, graphics buffering, and buffering
115 and image display on the projector). While it is hard to use GPU-based systems to reach
116 closed-loop delays below 100 ms (Stowers et al., 2017), simpler systems with direct LED control
117 allow for delays as short as 30 ms (Tadres and Louis, 2020).

118

119 Control experiments

120 Notably, animals navigating the "Constant" stimulus were always analyzed as if they navigated
121 the respective experimental stimulus ("Valley" or "Ramp"), using the same binning, naming
122 conventions, and analysis methods. For example, control animals that spend time in the "Dark"
123 ring (gray open circles in **Fig. 1D**) actually perceive constant gray during the entire experiment.
124 This analysis was chosen to control for the spatial arrangement of our stimulus and boundary
125 effects. The best example where this strategy is important can be seen for the turn-triggered
126 brightness change (**Fig. 2G**): Even though control animals always perceive gray, the turn-
127 triggered brightness dynamics indicate a complex dependency on the spatial arrangement of
128 the arena. Only by using this control analysis is it possible to appreciate the dynamics in the
129 experimental group.

130

131 Data analysis and statistics

132 All data analysis was performed using custom-written Python code on the 45 min period after
133 acclimatization. To avoid tracking problems and minimize boundary effects, data were excluded
134 where larvae were within 0.1 cm distance to the edge.

135 The circular arena was binned in three concentric regions depending on the radius r : $r = 0 -$
136 2 cm , $r = 2 - 4\text{ cm}$, and $r = 4 - 6\text{ cm}$. These regions were named the “Bright” center, the “Dark”
137 ring, and the “Bright” ring for the “Valley” stimulus (**Fig. 1B**) and the “Dark” center, the “Gray”
138 ring, and the “Bright” ring for the “Ramp” stimulus (**Fig. S3A**). Animal speed was computed by
139 interpolating the trajectory to 1 s bins and then by taking the average distance of consecutive
140 points (**Fig. 1E**).

141 For the turn event-based offline analysis (**Fig. 2**), a pose estimation toolbox, DeepPoseKit
142 (Graving et al., 2019), was used. To this end, 100 frames were manually annotated (head,
143 centroid, and tail) to train the neural network, which was then used to predict animal posture
144 across all frames from all animals. Body curvature was defined as the angle between the tail-to-
145 centroid vector and the centroid-to-head vector (**Fig. 2A**). The pose estimation algorithm
146 occasionally had difficulties distinguishing between the head and the tail. This problem was,
147 however, not relevant for the curvature measurement as the angle between these two body
148 parts does not change when they are flipped. In a few frames, the algorithm placed the head
149 and the tail at the same location, leading to the transient detection of large body curvatures.
150 These events were discarded by low-pass filtering traces with a Butterworth filter (cutoff
151 frequency: 3 Hz). Turn events were defined as a local curvature peak above 30° and needed to
152 be separated from the previous event by at least 2 s in time and 0.2 cm in space. The value for
153 the curvature threshold was chosen such that the identified curvature peaks clearly stood out
154 from the curvature fluctuations in between events (**Fig. 2A**).

155 Turn angles were defined as the angle between the location in the arena 2 s before a turn
156 event and 2 s after. Run-length was defined as the time between consecutive turn events. Each
157 turn event was labeled as “Dark” or “Bright”, based on the brightness equations and binning
158 described above (Dark: pixel brightness less than 29, Bright: otherwise), and as “Darkening” or
159 “Brightening” based on the sign in brightness change since the last turn event (**Fig. 2E,F**). As
160 turn events are short and spatially confined, by stimulus design, the whole-field brightness
161 change during such events is nearly zero (**Fig. 2D**). Notably, our curvature-based turn event
162 identification procedure does not allow for precise labeling of the beginning and the end of the

163 event. Therefore, the brightness change during turns was defined as the brightness difference
164 0.5 s before and 0.5 s after the event. This time range often includes brief periods of runs,
165 explaining the small residual width of the reported brightness distribution (**Figs. 2D and 3E**).
166 The brightness change during runs was defined as the difference in brightness between two
167 consecutive turn events (**Figs. 2D and 3E**).

168 Two-sample t-tests were used for pairwise comparisons between the experimental and
169 control data. Paired-sample t-tests were used for pairwise comparisons within groups. Statistics
170 for the linear regression fits (**Figs. S4A,B and S5A,B**) were based on a bootstrapping approach
171 by repeating the analysis 1000 times for shuffled data and then comparing the distribution of R^2
172 values to the one from the original dataset.

173 Larvae were discarded if they spent more than 99% of the experimental time in a single
174 region or if their speed was zero. All data analysis was done automatically in the same way for
175 the experimental and control groups.

176

177 Modeling

178 Simulations (**Figs. 3, S5, and S6**) were custom written in Python 3.7, using the high-
179 performance Python compiler numba. Simulations were performed using Euler's Method with a
180 timestep of $dt = 0.01$ s. Model larvae were initialized with a random position and orientation. At
181 each time step, larvae stochastically chose one of two possible actions: They could either move
182 forward, with a speed of 0.04 cm/s (parameter was taken directly from the experiment, **Fig. 1E**),
183 or turn. The baseline probability for turning was $p = 0.00066$. This value was directly computed
184 from the experiment to match the measured average run-length of $T = 15$ s (**Fig. 2E,F**),
185 following $p = dt / T$. When making turns, turn angles were drawn from a Gaussian distribution
186 with a baseline standard deviation of 32° , matching the experimental value (**Fig. 2C,E,F**). When
187 model larvae reached the edge, a new random direction vector was chosen, preventing them
188 from leaving the arena.

189 In correspondence with our experimental findings (**Fig. 2E,F**), the model was equipped with
190 four additional navigational rules (**Fig. 3A**).

191 "Rule 1": When the environment is "Dark" (brightness smaller than 29), turn angles
192 decrease. When it is "Bright" (brightness larger than 29), turn angles increase.

193 "Rule 2": When the environment is "Dark" (brightness smaller than 29), run-lengths increase.
194 When it is "Bright" (brightness larger than 29), run-lengths decrease.

195 “Rule 3”: When the environment is “Darkening” (change since previous turn smaller than
196 zero), turn angles decrease. When it is “Brightening” (change since previous turn larger than
197 zero), turn angles increase.

198 “Rule 4”: When the environment is “Darkening” (change since previous turn smaller than
199 zero), run-lengths increase. When it is “Brightening” (change since previous turn larger than
200 zero), run-lengths decrease.

201 Changes in turn angle were accomplished by adjusting the standard deviation of the
202 Gaussian distribution by $\pm 30\%$, the effect size observed in our experiments (**Fig. 2E,F**). We
203 modulated run-length (T) by scaling them by $\pm 30\%$, thereby modulating the probability of turning
204 ($p = dt / T$). When combinations of those rules were tested (**Fig. 3A**), effects were concatenated.

205 A performance index (PI) (**Fig. 3A**) was used to characterize how well animals or models
206 performed temporal phototaxis. The metric was based on the difference between the
207 experimental and control group for the fraction of time spent in the “Dark” ring. To compute this
208 value, bootstrapping was used to average 1000 samples of randomly chosen differences
209 between experimental and control conditions.

210 For the parameter grid search (**Fig. 3A**), the absolute turn angle and the run-length were
211 varied systematically. To this end, respective baseline parameter values (taken from the
212 experiment, **Fig. 2E,F**), were changed by scaling them with two multipliers (run-length multiplier
213 and turn angle multiplier).

214 Data generated from model larvae were analyzed and displayed using the exact same
215 scripts that were used to analyze experimental data, allowing for easy comparison between
216 model and animal behavior.

217

218 **Results**

219

220 Fly larvae can navigate a virtual brightness gradient

221 We first asked whether fly larvae can perform temporal phototaxis, i.e. navigate a virtual light
222 landscape lacking spatial information. We placed individual animals in an agarose-filled arena,
223 allowed them to freely explore, and tracked their position in real-time (**Fig. 1A**). We presented
224 spatially uniform light from below, with brightness levels following a quadratic dependence of the
225 larva's distance from the center ("Valley" stimulus, **Fig. 1B**) or constant gray as a control
226 ("Constant" stimulus). For both groups, we analyzed how animals distribute across three
227 concentric regions: the "Bright" center, the "Dark" ring, and the "Bright" ring. Notably, throughout
228 this study control animals were always analyzed as if they navigated the experimental stimulus
229 even though they in fact perceived constant gray. This analysis is important to control for the
230 spatial arrangement of our stimulus and boundary effects.

231 Larvae that navigated the "Valley" stimulus spent a significantly higher fraction of time in the
232 "Dark" ring than those that navigated the "Constant" stimulus (**Figs. 1C,D** and **S2B**). This
233 behavior was most pronounced between minutes 10 and 40 of the experiment (**Fig. S2C**). To
234 verify that this behavior was not an artifact of our specific stimulus design, we also tested a
235 gradient where brightness monotonically "ramps" with radial distance (**Fig. S3A**) and observed
236 that larvae also here navigated to dark regions (**Fig. S3B,C**).

237 Because larvae lacked spatial brightness cues in our setup, it was unclear which behavioral
238 algorithms they employ. One basic, yet potentially sufficient, algorithm would be to reduce
239 movement in darker regions. However, speed was independent of brightness (**Figs. 1E** and
240 **S3D**), suggesting that larvae employ more complex navigational strategies.

241 We conclude that *Drosophila* larvae are capable of performing phototaxis in the absence of
242 spatial information and that this behavior cannot be explained by a simple brightness-dependent
243 modulation of crawling speed.

244

245 Larval temporal phototaxis depends on brightness change over time

246 In spatially differentiated light landscapes, fly larvae make navigational decisions by sampling
247 brightness differences during head-casts. In our setup, by design, larvae experience no
248 brightness fluctuations during head-casts. Hence, they have to use whole-field brightness or
249 brightness history information to modulate the magnitude and/or frequency of turns. To explore

250 this possibility, we segmented trajectories into runs and turns. We applied a deep learning-
251 based package, DeepPoseKit (Graving et al., 2019) to extract the larvae's head, centroid, and
252 tail positions from the experimental video (**Fig. 2A** and **Video S2**). From there, we calculated
253 the animal's body curvature to identify head-casting events and to quantify turn angles and run-
254 lengths (**Fig. 2A–C**).

255 As expected, brightness changes during the spatially confined turns were negligible
256 compared to ones measured during runs (**Fig. 2D**). To quantify the effect of brightness on
257 heading angles and run-lengths, we checked how these parameters varied with the larva's
258 position. During the "Valley" but not the "Constant" stimulus, turns in the "Dark" region led to
259 smaller heading angle changes than in the "Bright" regions (**Fig. 2E**). Similarly, runs before a
260 turn in the "Dark" region of the "Valley" stimulus were slightly longer compared to runs ending in
261 the "Bright" region. However, this also partly occurred with the "Constant" stimulus, suggesting
262 that the effect might not arise from a visuomotor transformation.

263 Next, we explored whether brightness history affects behavior. As run-lengths were highly
264 variable, ranging from ~3 s to ~40 s (**Fig. 2C**), we focused our analysis on the brightness
265 change between consecutive turns. We classified turns by whether larvae experienced a
266 decrease or increase in whole-field brightness during the preceding run. We found that heading
267 angle changes were smaller and that run-lengths were longer when larvae had experienced a
268 brightness decrease compared to an increase (**Fig. 2F**). We did not observe these effects in
269 control animals.

270 To further quantify the effects of brightness and brightness change on heading angle
271 change, we performed regression analysis directly on individual events (**Fig. S4**). While turn
272 angles scale with brightness, they do so more strongly with brightness change.

273 These observations led us to hypothesize that larvae might integrate information about the
274 change in brightness during runs and that this integration period might span several seconds.
275 To obtain an idea about time-scales, we computed a turn event-triggered brightness average
276 (**Fig. 2G**). We observed that, on average, turns performed in the "Valley" stimulus are preceded
277 by an extended period of >20 seconds of brightening, suggesting that long-term brightness
278 increases drive turns.

279 In summary, our analysis of turns and runs confirms that, first, brightness levels modulate
280 heading angle change and, second, changes in brightness prior to turns modulate heading
281 angle change as well as run-length.

282

283 A simple algorithmic model can explain larval temporal phototaxis

284 We next wanted to test whether the identified behavioral features are sufficient to explain larval
285 temporal phototaxis. Based on our experimental findings (**Fig. 2**), we propose four rules as
286 navigational strategies (**Fig. 3A**). For rules 1 and 2, the instantaneous brightness modulates the
287 heading angle change and run-length, respectively. By contrast, for rules 3 and 4, the
288 brightness change since the last turn modulates the heading angle changes and run-lengths.

289 To test these navigational rules, we simulated larvae as particles that could either move
290 straight or make turns. To compare the performances of different models, we calculated a
291 phototaxis index (difference of time spent in the “Dark” ring between experimental and control
292 groups, **Fig. 3A**). For all permutations of our rules, we explored a set of multipliers for the
293 heading angle change and run-length, with a multiplier of 1 corresponding to the experimental
294 averages (**Fig. 2E,F**). This allowed us to assess the robustness of our model to parameter
295 choice. As expected, with no active rules, the larval distribution was comparable between the
296 “Valley” and “Constant” stimulus. Activating rules 1 or 2, performance did not improve,
297 suggesting that modulation of behavior based on instantaneous brightness is insufficient to
298 perform temporal phototaxis. Activating rules 3 or 4, phototaxis emerged for small run-lengths
299 and large turn angle multipliers. However, for multipliers set to 1, the resulting phototaxis index
300 was weaker than in experiments (= 14 %). Only when combining rules 3 and 4, phototaxis
301 performance matches the experimental values. Combining all four rules yielded minimal
302 improvements. Therefore, for further analysis, we focused on a combination of rules 3 and 4,
303 with both multipliers set to 1.

304 Like real larvae (**Fig. 1C–E**), simulated larvae navigating the “Valley” stimulus spent more
305 time in the “Dark” ring than larvae navigating the “Constant” stimulus (**Fig. 3B,C**) without
306 modulating speed (**Fig. 3D**). Furthermore, distributions of turn angle changes, run-lengths, and
307 brightness changes were comparable to experimental data (compare **Figs. 2C,D** and **3E,F**).
308 Residual differences in those distributions are likely due to additional mechanisms used by the
309 animal, such as a refractory period for turn initiation, which we did not incorporate in our model.
310 When we examined the effects of instantaneous brightness and brightness change on turn
311 angle amplitude and run-length (**Fig. 3G,H**), we observed similar patterns as in the experimental
312 data (**Fig. 2E,F**). As found in experiments (**Fig. 2G**), turns are preceded by long stretches of
313 increasing brightness (**Fig. 3I**), supporting our hypothesis that larvae integrate brightness
314 change over several seconds. Moreover, in the event-based regression analysis we found
315 results to be in agreement with experimental data as well (compare **Figs. S4** and **S5**). Finally, to

316 verify that our model generalizes to other visual stimulus patterns, we simulated larvae exploring
317 the “Ramp” stimulus and observed phototaxis performance comparable to that of real larvae
318 (compare **Figs. S3** and **S6**).

319 In summary, after implementing our experimentally observed navigational rules in a simple
320 computational model, we propose that the most critical element of larval temporal phototaxis is
321 the ability to integrate brightness change over extended time periods. Modulating turn angle
322 amplitude and run-length based on such measurement is sufficient to perform temporal
323 phototaxis.

324

325 Discussion

326 Using a closed-loop behavioral assay, we show that *Drosophila* larvae find the darker regions of
327 a virtual brightness gradient that lacks any spatial contrast cues. Temporal phototaxis
328 behavioral algorithms have already been dissected in open-loop configurations, where stimuli
329 are decoupled from an animal's actions. Following a global brightness increase, larvae are
330 known to modify both their heading angle magnitude and their run-length (Gepner et al., 2015;
331 Kane et al., 2013), which is in agreement with our findings. We were able to demonstrate that
332 these navigational strategies are in fact sufficient for phototactic navigation. Given that
333 brightness fluctuations in our assay are slow and negligibly small during head-casts, we suggest
334 that animals integrate brightness change during runs to make decisions about the strength and
335 timing of turns. Previous work has shown that larvae can navigate olfactory or thermal gradients
336 using only temporal cues (Luo et al., 2010; Schulze et al., 2015). Together with our findings, this
337 should enable future exploration of the shared computational principles and neural pathways
338 across these sensory modalities.

339 Closed-loop systems are powerful tools to dissect an animal's sensorimotor transformation.
340 They have been employed in many models including adult *Drosophila* (Bahl et al., 2013), larval
341 zebrafish (Bahl and Engert, 2020; Chen and Engert, 2014), and *C. elegans* (Kocabas et al.,
342 2012; Leifer et al., 2011). Recent work in *Drosophila* larvae used LED-based devices to study
343 closed-loop temporal chemotaxis in virtual optogenetic environments (Tadres and Louis, 2020).
344 Such systems are cheaper and have shorter stimulus refresh times but cannot easily be used to
345 present animals with spatially differentiated landscapes. By utilizing a projector, our setup
346 overcomes this limitation. With the drawback of slightly longer delays and higher component
347 costs, the ability to present any type of visual stimulus adds important flexibility and versatility.

348 Future studies could use our paradigm to study, for example, specific behavioral differences
349 between animals navigating a true luminance gradient compared to when they navigate the
350 exact same one virtually. Moreover, our system makes it possible to explicitly investigate
351 navigational strategies exclusively using spatial information. This has already been achieved in
352 zebrafish larvae (Chen et al., 2020; Huang et al., 2013) by always locking a sharp contrast edge
353 to the center of the animal's head. Testing such stimuli in *Drosophila* larvae will, however,
354 require more precise real-time position, orientation, and posture measurements, improvements
355 that can be added to our setup. The result from such experiments could be used to construct a
356 spatial phototaxis model which could then be combined with our proposed temporal phototaxis
357 model.

358

359

360 **Acknowledgments**

361 We thank L. Hernandez-Nunez for discussions and reading through the manuscript. We are
362 grateful to F. Engert and A. Samuel and their lab members for discussions and general support.

363

364 **Author contributions**

365 All authors contributed equally to the design of the project. A.B. built the behavioral setup. M.Z.
366 performed experiments. M.Z. and A.B. analyzed data. M.Z., K.J.H., K.V., and A.B. wrote the
367 manuscript. K.J.H., K.V., and A.B. supervised the work.

368

369 **Competing interests**

370 The authors declare no competing interests.

371

372 **Funding**

373 K.J.H. was funded by the Harvard Mind Brain Behavior Initiative. K.V. received funding from a
374 German Science Foundation Research Fellowship #345729665. A.B. was supported by the
375 Human Frontier Science Program Long-Term Fellowship LT000626/2016. We thank the
376 Zukunftskolleg Konstanz for supporting A.B.

377

378 **Data availability**

379 The data that support the findings of this study are available from the corresponding author
380 upon request. Source code for data analysis and modeling are available on GitHub
381 (https://github.com/arminbahl/drosophila_phototaxis_paper).

382

383 **References**

384

385 **Bahl, A. and Engert, F.** (2020). Neural circuits for evidence accumulation and decision making
386 in larval zebrafish. *Nat. Neurosci.* **23**, 94–102.

387 **Bahl, A., Ammer, G., Schilling, T. and Borst, A.** (2013). Object tracking in motion-blind flies.
388 *Nat. Neurosci.* **16**, 730–738.

389 **Chen, X. and Engert, F.** (2014). Navigational strategies underlying phototaxis in larval
390 zebrafish. *Front. Syst. Neurosci.* **8**, 1–13.

391 **Chen, A. B., Deb, D., Bahl, A. and Engert, F.** (2020). Algorithms underlying flexible phototaxis
392 in larval zebrafish. *bioRxiv* 2020.07.18.210260.

393 **Gepner, R., Mihovilovic Skanata, M., Bernat, N. M., Kaplow, M. and Gershow, M.** (2015).
394 Computations underlying *Drosophila* photo-taxis, odor-taxis, and multi-sensory integration.
395 *Elife* **4**, 1–21.

396 **Gomez-Marin, A. and Louis, M.** (2012). Active sensation during orientation behavior in the
397 *Drosophila* larva: more sense than luck. *Curr. Opin. Neurobiol.* **22**, 208–215.

398 **Gomez-Marin, A. and Louis, M.** (2014). Multilevel control of run orientation in *Drosophila* larval
399 chemotaxis. *Front. Behav. Neurosci.* **8**, 1–14.

400 **Gomez-Marin, A., Stephens, G. J. and Louis, M.** (2011). Active sampling and decision making
401 in *Drosophila* chemotaxis. *Nat. Commun.* **2**, 1–10.

402 **Graving, J. M., Chae, D., Naik, H., Li, L., Koger, B., Costelloe, B. R. and Couzin, I. D.**
403 (2019). DeepPoseKit, a software toolkit for fast and robust animal pose estimation using
404 deep learning. *Elife* **8**, e47994.

405 **Huang, K.-H., Ahrens, M. B., Dunn, T. W. and Engert, F.** (2013). Spinal projection neurons
406 control turning behaviors in zebrafish. *Curr. Biol.* **23**, 1566–1573.

407 **Humberg, T.-H. and Sprecher, S. G.** (2018). Two pairs of *Drosophila* central brain neurons
408 mediate larval navigational strategies based on temporal light information processing.
409 *Front. Behav. Neurosci.* **12**, 1–6.

410 **Humberg, T.-H., Bruegger, P., Afonso, B., Zlatic, M., Truman, J. W., Gershow, M., Samuel,**
411 **A. and Sprecher, S. G.** (2018). Dedicated photoreceptor pathways in *Drosophila* larvae
412 mediate navigation by processing either spatial or temporal cues. *Nat. Commun.* **9**, 1–16.

413 **Kane, E. A., Gershow, M., Afonso, B., Larderet, I., Klein, M., Carter, A. R., de Bivort, B. L.,**
414 **Sprecher, S. G. and Samuel, A. D. T.** (2013). Sensorimotor structure of *Drosophila* larva
415 phototaxis. *Proc. Natl. Acad. Sci. U.S.A.* **110**, 3868–3877.

416 **Klein, M., Afonso, B., Vonner, A. J., Hernandez-Nunez, L., Berck, M., Tabone, C. J., Kane,**
417 **E. A., Pieribone, V. A., Nitabach, M. N., Cardona, A., et al.** (2015). Sensory determinants
418 of behavioral dynamics in *Drosophila* thermotaxis. *Proc. Natl. Acad. Sci. U.S.A.* **112**, 220–
419 229.

- 420 **Kocabas, A., Shen, C.-H., Guo, Z. V. and Ramanathan, S.** (2012). Controlling interneuron
421 activity in *Caenorhabditis elegans* to evoke chemotactic behaviour. *Nature* **490**, 273–277.
- 422 **Lahiri, S., Shen, K., Klein, M., Tang, A., Kane, E., Gershow, M., Garrity, P. and Samuel, A.**
423 **D. T.** (2011). Two alternating motor programs drive navigation in *Drosophila* larva. *PLoS*
424 *One* **6**, 1–12.
- 425 **Leifer, A. M., Fang-Yen, C., Gershow, M., Alkema, M. J. and Samuel, A. D. T.** (2011).
426 Optogenetic manipulation of neural activity in freely moving *Caenorhabditis elegans*. *Nat.*
427 *Methods* **8**, 147–152.
- 428 **Luo, L., Gershow, M., Rosenzweig, M., Kang, K., Fang-Yen, C., Garrity, P. A. and Samuel,**
429 **A. D. T.** (2010). Navigational decision making in *Drosophila* thermotaxis. *J. Neurosci.* **30**,
430 4261–4272.
- 431 **Mazzoni, E. O., Desplan, C. and Blau, J.** (2005). Circadian pacemaker neurons transmit and
432 modulate visual information to control a rapid behavioral response. *Neuron* **45**, 293–300.
- 433 **Sawin, E. P., Harris, L. R., Campos, A. R. and Sokolowski, M. B.** (1994). Sensorimotor
434 transformation from light reception to phototactic behavior in *Drosophila* larvae (Diptera:
435 Drosophilidae). *J. Insect Behav.* **7**, 553–567.
- 436 **Sawin-McCormack, E. P., Sokolowski, M. B. and Campos, A. R.** (1995). Characterization
437 and genetic analysis of *Drosophila melanogaster* photobehavior during larval development.
438 *J. Neurogenet.* **10**, 119–135.
- 439 **Schulze, A., Gomez-Marin, A., Rajendran, V. G., Lott, G., Musy, M., Ahammad, P.,**
440 **Deogade, A., Sharpe, J., Riedl, J., Jarriault, D., et al.** (2015). Dynamical feature
441 extraction at the sensory periphery guides chemotaxis. *Elife* **4**, e06694.
- 442 **Stowers, J. R., Hofbauer, M., Bastien, R., Griessner, J., Higgins, P., Farooqui, S., Fischer,**
443 **R. M., Nowikovskiy, K., Haubensak, W., Couzin, I. D., et al.** (2017). Virtual reality for
444 freely moving animals. *Nat. Methods* **14**, 995–1002.
- 445 **Tadres, D. and Louis, M.** (2020). PiVR: An affordable and versatile closed-loop platform to
446 study unrestrained sensorimotor behavior. *PLoS Biol.* **18**, e3000712.
- 447

448 **Figure legends**

449

450 **Figure 1. *Drosophila* larvae can perform temporal phototaxis.** (A) Setup for tracking freely-crawling
451 *Drosophila* larvae. (B) Whole-field pixel brightness versus larval position for the “Valley” and “Control”
452 stimulus. (C) Raw trajectories. Dashed circles delineate the “Bright” center, the “Dark” ring, and the
453 “Bright” ring. (D) Fraction of time spent in regions (left to right: $p = 0.045$, $p = 0.001$, $p < 0.001$; two-sided
454 t-tests). (E) Crawling speed in regions (left to right: $p = 0.304$, $p = 0.891$, $p = 0.479$; two-sided t-tests).
455 Error bars represent mean \pm SEM. Blue solid lines and dots indicate “Valley” stimulus larvae; gray solid
456 lines and dots indicate “Constant” stimulus larvae. $N = 27$ larvae for both groups. Open small circles
457 represent individual animals.

458

459 **Figure 2. Brightness and brightness history modulate navigational decisions.** (A) Posture tracking
460 for estimating larval body curvature (angle between solid and dashed blue lines). Turns (orange circles)
461 are curvature peaks above a threshold (30°). (B) Example trajectory with detected turns for an inset view
462 (top) and the entire arena (bottom). (C,D) Probability density distributions for turn angles and run-length
463 (C) and respective brightness changes (D). (E,F) Turn angle and run-length as a function of light intensity
464 (dark: < 29 ; bright: otherwise; see brightness profile, **Fig. 1B**) and as a function of brightness change
465 since the previous turn (left to right: $p = 0.004$, $p = 0.010$, $p < 0.001$, $p = 0.006$ for the “Valley” stimulus
466 and $p = 0.289$, $p = 0.018$, $p = 0.066$, $p = 0.221$ for the “Constant” stimulus; paired t-tests). (G) Turn event-
467 triggered brightness for the “Valley” and the “Constant” stimulus (mean \pm SEM over all turns from all
468 larvae, $n = 3153$ and $n = 2981$ turns, respectively). $N = 27$ larvae for both groups. Open small circles and
469 thin solid lines in (E,F) represent median turn angle and run-length for individual larvae.

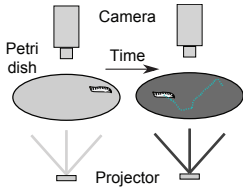
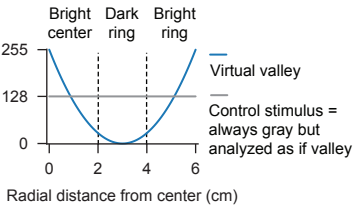
470

471 **Figure 3. Simulated larvae perform temporal phototaxis.** (A) Characterization of combinations of four
472 potential navigational rules, with a grid search for the parameters run-length and turn angle, quantified by
473 a phototaxis performance index. (B–I) Simulations using only Rules 3 and 4, with turn angle and run-
474 length multiplier set to one. (B–D) Raw trajectories, fraction of time spent in regions, and crawling speed
475 (as in **Fig. 1C–E**). Left to right: (C) $p = 0.181$, $p < 0.001$, $p = 0.015$; two-sided t-tests; (D) $p = 0.531$, $p =$
476 0.651 , $p = 0.665$; two-sided t-tests. (E–I) Analysis of turns and runs (as in **Fig. 2C–G**). (G,H) Left to right:
477 $p < 0.001$, $p = 0.001$, $p < 0.001$, $p < 0.001$ for the “Valley” stimulus; $p = 0.283$, $p = 0.165$, $p = 0.796$, $p =$
478 0.656 for the “Constant” stimulus; paired t-tests. Open circles and thin solid lines in (C–I) represent
479 individual model larvae. $N = 50$ simulation runs for both groups using different random seeds. $N = 5331$
480 and $n = 5334$ events in (I).

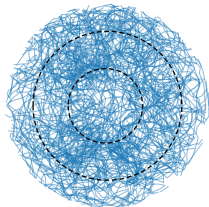
481

A

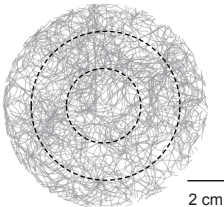
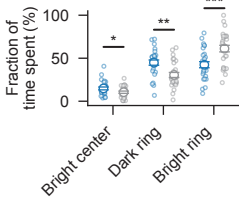
Experimental setup

**B**Whole-field brightness
(in pixel value units)**C**

Virtual valley



Control (always gray)

**D****E**